

# Determining Planck's constant using a Tungsten Filament lamp

Sara Capdevila Solé, CID: 01727810.

**Abstract**—The light emission spectrum from a Tungsten filament lamp has been investigated for five different wavelengths in the visible range;  $(560 \pm 8)\text{nm}$ ,  $(552 \pm 11)\text{nm}$ ,  $(500 \pm 8)\text{nm}$ ,  $(457 \pm 10)\text{nm}$  and  $(400 \pm 9)\text{nm}$ . Measurements were recorded with a Silicon photodetector in the temperature range of emission of  $[1, 2] \times 10^3\text{K}$ , which was found indirectly through a Wheatstone bridge setup. Under the assumption that the filament bulb can be modelled as a blackbody, using Planck's law, values for  $h$  can be extracted. An average value of  $h = (4.84 \pm 0.13) \times 10^{-34}\text{Js}$  is obtained, which is 27% lower than the theoretical value of  $h = 6.626 \times 10^{-34}\text{Js}$ . We empirically model and visualise the light distribution along the filament. Findings suggest our values of  $h$  are underestimates; as the light mainly propagates from the hottest central part of the filament. Finally, we discuss other implications affecting our results and further improvements to this investigation.

## I. INTRODUCTION

IN March of 1858 Balfour Stewart presented to the Royal Society of Edinburgh the first experiments involving the investigation of various materials as absorbers and emitters of radiant heat. However, it wasn't until 1859, that Gustav Kirchhoff formulated a thermodynamic derivation. The idea of a black body was proposed in his theory [1];

"The supposition that bodies can be imagined which, for infinitely small thicknesses, completely absorb all incident rays, and neither reflect nor transmit any. I shall call such bodies perfectly black, or, more briefly, black bodies"

Following this formulation, in 1896 Wilhelm Wien empirically determined a distribution law of blackbody radiation, relating the spectral radiance of a body to the exponential of the temperature of the body times some constant [2]. It wasn't until the 1900s, that Max Planck used electromagnetism and thermodynamics to propose a theoretical basis for Wien's law, which included a new fundamental constant called Planck's constant  $h = 6.62607015 \times 10^{-34}\text{Js}$  [3].

Blackbody theory can be applied to many areas of physics. It can be used to investigate cosmological phenomena, such as relativistic doppler shifts in moving galaxies, the nature of cosmic microwave background radiation, as well as black holes and their theoretical black body (hawking) radiation [4].

In this report, we apply this blackbody theory to a tungsten filament lamp, by measuring its intensity spectrum at different temperatures in 5 different wavelengths. We discuss the theoretical and empirical methodology used to derive a value of  $h$ . Additionally, we evaluate and discuss possible improvements and limitations to our methods.

## II. THEORY

### A. Blackbody radiation

The spectral radiance  $I_B$  emitted by a blackbody can be modelled with Planck's law [5],

$$I_B(\lambda, T) = \frac{2hc^2}{\lambda^5} \frac{1}{e^{(hc/\lambda k_B T)} - 1}. \quad (1)$$

The spectrum depends on the temperature  $T$  of the source, emitting light at a wavelength  $\lambda$ . The fundamental constants  $c$ ,  $h$  and  $k_B$  are the speed of light, Planck's constant and Boltzmann's constant respectively.

In the limit of high frequencies, Wein's approximation rewrites  $I_B$  using  $hc \gg \lambda k_B T$  as

$$I_B(\lambda, T) = \frac{2hc^2}{\lambda^5} \exp\left(-\frac{hc}{\lambda k_B T}\right). \quad (2)$$

In this investigation we use  $T < 2000\text{K}$  and  $\lambda < 600\text{nm}$ , which makes this approximation suitable.

### B. Voltage-Temperature dependence

The incoming flux from the source (lamp) is  $\Phi \propto \int I_B \delta\lambda$ . Additionally, using a photodetector with response  $V$ , it will satisfy  $\Phi \propto V$  if used in its linear region [6].

When a filter  $f(\lambda)$  is placed in the setup, the resulting voltage  $V_f$  is a convolution of the spectrum and the filter; with centre wavelength  $\lambda_0$  and bandwidth  $\Delta\lambda$ ,

$$V_f \propto \int_0^{+\infty} I_B(\lambda', T) f(\lambda') d\lambda'. \quad (3)$$

Under the assumption that the filter can be approximated to a top-hat function centred at  $\lambda_0$ , with width  $2\Delta\lambda$ , the integral is

$$V_f \propto \int_{\lambda_0 - \Delta\lambda}^{\lambda_0 + \Delta\lambda} \exp\left(-\frac{hc}{\lambda' k_B T}\right) \frac{d\lambda'}{\lambda'^5} \quad (4)$$

Solving (4) assuming a very narrow bandwidth  $\Delta\lambda \ll \lambda$ , results in  $V_f \propto \exp(-\frac{hc}{\lambda k_B T})$ .

Taking the logarithm of the expression gives

$$\ln(V) = -\frac{hc}{\lambda_0 k_B T} + C, \quad (5)$$

where  $C$  is a constant, dependent on the angular parameter from the spectrum's dispersion and the photodetector amplifier response.

### C. Tungsten

Tungsten is a metal with the highest melting point  $T \approx 3695\text{K}$ . It has been studied widely since the beginning of the 20th century, due to its varied properties, such as the production of filaments in incandescent lamps [7].

Equation (1) needs to be modified for non-perfect blackbodies, also called grey bodies, by introducing the bodies emissivity  $\epsilon$  which is less than unity. This results in  $I_G(\lambda, T) = \epsilon(\lambda, T)I_B(\lambda, T)$ . Nonetheless, if this factor is constant and independent of  $\lambda$  or  $T$ , the spectral distribution is unchanged from a blackbody and we can use (1) directly. Worthing et al. [8] finds that at a given  $\lambda$ ,  $\epsilon$  has a decreasing value with  $T$ . In this investigation, given the range of  $\lambda$  and  $T$  used, we assume the tungsten emissivity is constant and treat it as a blackbody.

#### 1) Tungsten filament

A lamp containing tungsten filament was used in this experiment. Stefan-Boltzmann's law states that the energy flux emitted by a black body is  $\propto T^4$  [2]. The main form of heat dissipation by the Joule effect is heat transfer (radiative and convective being negligible at these low temperatures). At a steady-state, where the temperature is uniform across the diameter, this heat source will be dominated by the hottest part of the filament (around the centre). Through digital processing, we can image, analyse the light distribution along the filament. This will allow us to extract the typical length over which the temperature of the filament varies, as a function of temperature: the characteristic length  $z(T)$ . This relationship is expected to be linear [7] [9].

### D. Finding Planck's constant

Since the filament of the lamp is essentially a resistance heated by the Joule effect, we can measure the variation in resistance of the lamp  $R$  as we pass more current through it and deduce a variation with the received detection voltage  $V$  at the photodetector.

Plotting  $\ln(V)$  against  $1/T$  allows us to determine the value of  $h$  from its gradient.

## III. EXPERIMENTAL SETUP

#### 1) Tungsten lamp

A standardised tungsten lamp filament from Thorlabs [10] is used to model a blackbody spectrum in this experiment. The precise lamp used is shown in Fig. 1.

The emissivity correction for tungsten from [8], shows significant variations of  $\epsilon$  for short  $\lambda < 0.5\mu\text{m}$  at small  $T < 1800\text{ K}$ . Obtaining data for these values was not possible, due to the unreliable, weak signal received at the detector. In the other regions of  $\lambda$  and  $T$ ,  $\epsilon$  is fairly constant, with a maximum variation  $\Delta\epsilon = 2\%$ . As a result, the emissivity of tungsten was taken to be constant at  $\epsilon \approx 0.46 \pm 0.1$ . This allows us to model the filament as a blackbody and use (5).

### A. Optical setup

Fig. 2 shows the experimental setup used to measure the dependence of  $T$  of the lamp with the output  $V$  received at



Fig. 1: **Tungsten lamp:** A 12V-rated Thorlabs' Quartz Tungsten-Halogen filament lamp is used in this experiment. The coiling shape of the filament is portrayed in the image. This picture was taken with an iPhone X.

the detector. The lamp rays went through a variable iris so that they could be modelled as an isotropic point source, reducing the amount of light received from inner-glass reflections. Particular wavelengths were filtered using a spectral filter. The rays were focused using a convex lens onto a Silicon photodetector.

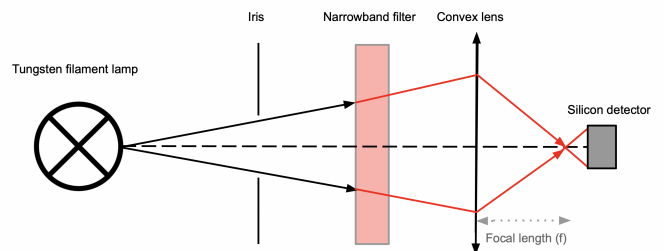
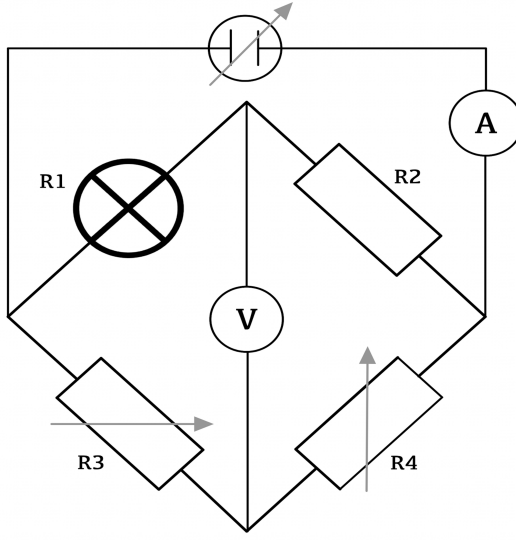


Fig. 2: **Schematic of the optical setup:** A Thorlabs' Quartz tungsten-halogen filament lamp was placed inside a bulb casing, and connected to a power supply. The rays emitted from the lamp go through a variable iris, which reduces the amount of reflection received from the back of the bulb glass. These rays consecutively enter 1 of the 5 narrowband interference filters (these are in the visible range; red, orange, green, blue, violet), and are sequentially focused (at  $f$ ) using a convex lens onto a Silicon ( $Si$ ) photodetector. The detector is connected to a multimeter. All of these components were placed on an optical train.

The setup was blacked out with an opaque cloth to reduce the light pollution coming from the lab room reaching our photodetector.

### 1) The Wheatstone bridge

The tungsten bulb with resistance  $R_1$  was placed in a Wheatstone bridge circuit with three other resistors ( $R_i$  with  $i = 2, 3, 4$ ), as shown in Fig. 3.



**Fig. 3: Wheatstone bridge:** A series of 4 resistors  $R_i$  with  $i = 1, 2, 3, 4$ . This electrical setup is used to measure the temperature  $T$  of the tungsten filament lamp ( $R_1$ ), at different currents supplied, measured using an ammeter  $A$ . The variables resistors can be adjusted such that there's no current flowing between the two branches (i.e. voltage  $V = 0\text{V}$ ).

Fixing  $R_2$  and  $R_4$ , allows us to vary  $V$  by adjusting only  $R_3$ . When no current flows through both branches ( $V = 0\text{V}$ ), we can determine the value of  $R_1$  as a function of the other resistances,

$$R_1 = \frac{R_2 R_3}{R_4}. \quad (6)$$

Using this equation, we can find the temperature  $T$  of the tungsten lamp, given a conversion relation  $T(R_1)$ .

### B. Detectors

The detector used in this investigation was a Thorlabs Silicon Amplified Photodetector, with a  $V$  response between  $[0, 10]\text{V}$  and an amplification in the range of  $[0, 70]\text{dB}$ . This detector may saturate both ends of its response curve.

Additionally, a Complementary Metal Oxide Semiconductor (CMOS) camera was used for the image analysis in Section V-A. This allowed us to study the light distribution projected from the tungsten filament lamp.

## IV. PRELIMINARY RESULTS

Care was taken to reduce overheating by turning off the setup between runs, as well as ensuring the detector response wasn't saturated or contaminated by ambient light, which was limited to the order of a couple of  $\text{mV}$ . Additionally, we made sure the spectral filters were normal to the optical setup, to reduce the diffraction of the incident rays. A slight deviation in this angle  $\Delta\theta \approx 10^\circ$  could shift our value of  $\lambda_0$  by  $\approx 2\text{nm}$ .

Furthermore, we ensured that the filtered beam was focused directly into the detector, and had the same size (these were matched by adjusting the iris).

The data was acquired by increasing the current of the power supply or by decreasing it, starting from an initially high current, and calculating the average. This was done slowly to help ensure the filament had reached a steady-state and was adequately emitting at the temperature we were expecting. The value of  $R_2$  has a fixed value of  $1\Omega$ , and  $R_4$  was set at the maximum possible setting of  $122\text{k}\Omega$ .

### A. Linearity of photodetectors

In order to use (5), we had to ensure our light rays were incident into the silicon detector, at the focal length of the bi-convex lens (as shown in Fig. 2). Using red light the focal length of the lens was measured at  $f = (9.8 \pm 0.1)\text{cm}$ . This is the range where our detectors' intensity response will be linear and we will observe an inverse-square law, as we move the detector a distance  $d$  away from  $f$ . This is due to the approximately isotropic nature of the point source. This relationship is plotted in Fig. 4.

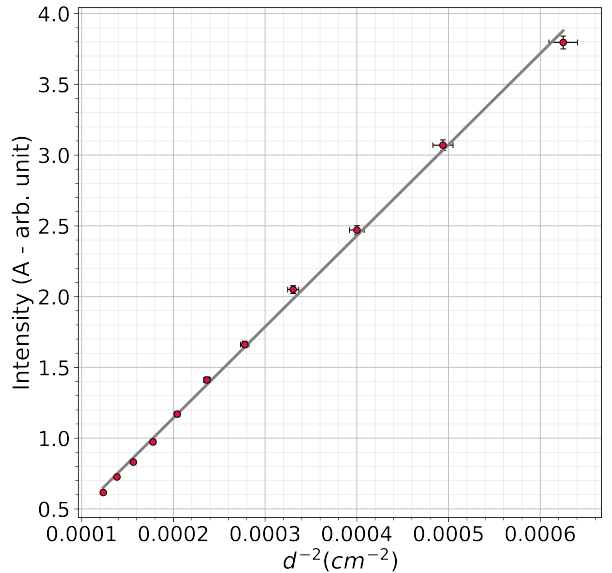


**Fig. 4: Linear response of detector:** By moving detector a distance  $d$  away from the focal length  $f$  of the bi-convex converging lens, we observe the expected inverse square relationship of  $1/d^2$ . This means we are using the detector in its region of linear response and we are not saturating it. These measurements are obtained using the red narrowband filter of  $600\text{nm}$  (red) at an amplification of  $70\text{dB}$ .

### B. Filters

The narrowband filters were measured using a high-precision characterisation system (Optical Spectrum Analyzers and Compact CCD Spectrometers software; OSA) [10]. Their distributions were fitted with a gaussian, and the mean  $\lambda_0$  and FWHM  $\Delta\lambda$  were found. The data extracted from the software is presented in Fig. 5. Additionally, the values are summarised in Table I.

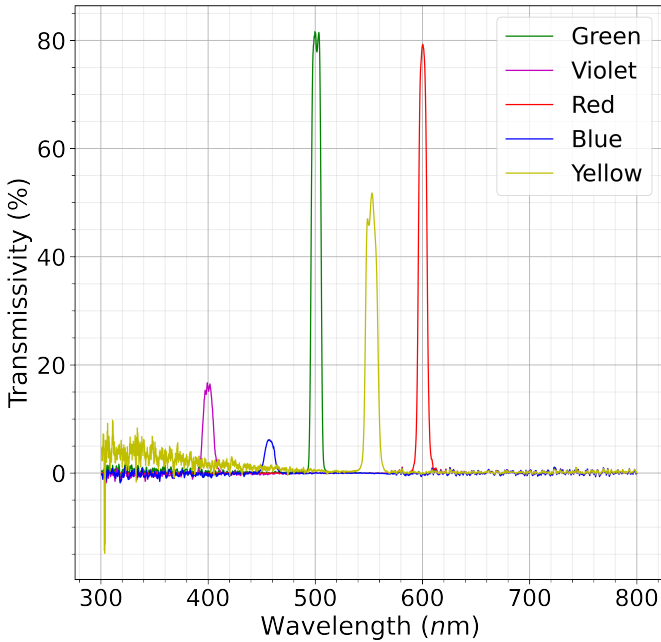


**Fig. 5: Filters characterisation using OSA:** Optical Spectrum Analyzers and Compact CCD Spectrometers software from Thor labs was used to extract the values of the centre wavelength  $\lambda_0$  and its bandwidth  $\Delta\lambda$  for each of the 5 filters.

Colour	$\lambda_0$ (nm)	$\Delta\lambda$ (nm)
Red	599.9	7.7
Yellow	552.1	10.6
Green	500.4	8.4
Blue	456.9	9.8
Violet	399.9	9.4

**TABLE I: Narrowband filters specification:** The centre wavelength  $\lambda_0$  and bandwidth  $\Delta\lambda$  of the 5 filters used and their corresponding colours in the visible spectrum. These results were extracted using Thorlabs OSA software, with an integration time of 1s.

Given the results, our narrowband approximation to derive (5) is reasonable. The values of  $\Delta\lambda$  are used for the uncertainty in  $\lambda_0$ .

### C. Temperature-Resistance conversion

Depending on the filament, the absolute resistance conversion  $R(T)$  will vary. To account for this, we infer its temperature  $T$  using its resistance relative to room temperature at  $T = 293K$ :  $R_{293}$ . The conversion data from the lab script [5], was extracted and interpolated by fitting a parabola using a least-squares method. The relative error in this fit is  $< 1\%$ .

$$R(T)/R_{293} = -0.593 + 0.00481T + 3.27 \times 10^{-7}T^2 \quad (7)$$

We compared with other parabolic fits from Izarra et al. [7] and Pawłowski [11]. These present a maximum difference of 3.9% to our fit, in the range of  $T$  of our obtained data. The three conversion relations and the deviation from the lab script (7) is plotted in Fig. 6.

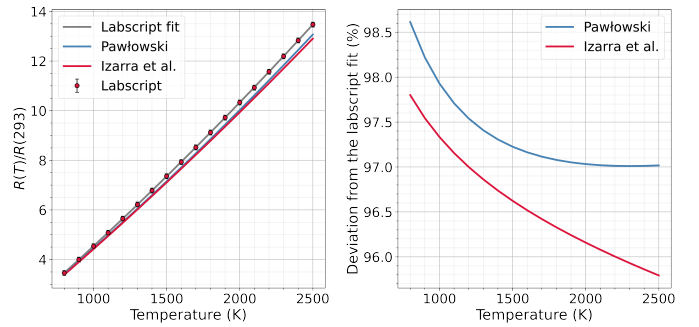


**Fig. 6: Resistance-Temperature relation:** The left plot shows the parabolic variation of  $R(T)/R_{293}$  from 3 different sources; Izarra et al. [7], Pawłowski [11] and the recommended data from the lab script [5]. The right plot shows the systematic % deviation of the two former sources with the latter.

The average percentage deviation of the two external sources from the lab script data is used later in our error analysis for  $h$ .

#### 1) Determining $R_{293}$

The value of  $R_{293}$  was determined in two different ways. Initially, we inferred it by extrapolated to zero current ( $I \rightarrow 0A$ ) using a parabolic model:  $R(I) = R_{293} + AI^2$ . This follows the assumption that at very low supplied current, the resistance from the filament is solely caused by the room heat (at  $T \approx 293K$ ). The results extracted are plotted in Fig. 7. This method gave us a value of  $R_{293} = (1.212 \pm 0.018)\Omega$ .

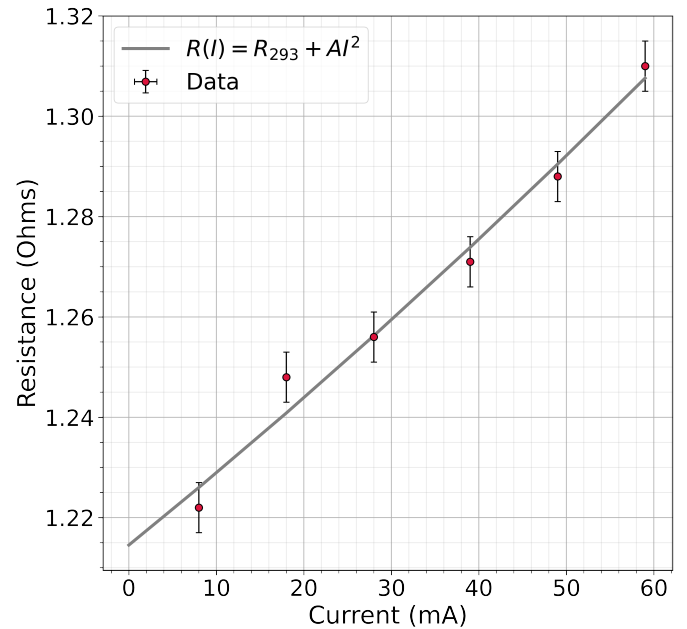


**Fig. 7: Determining  $R_{293}$ :** The first method of extracting the resistance of the tungsten filament at room temperature, by extrapolating the current to 0A using a quadratic fit.

Given that the current cannot be measured directly and that the resistances of the contacts and wires are significantly higher than that of the filament at room temperature, this value is expected to give an overestimate for  $R_{293}$ .

The second method of extracting  $R_{293}$  was using the blow-

up method. It is believed that this method gives a more accurate value [12]. By slowly raising and monitoring the voltage of the power supply to 24.6V, the bulb rated for 12V and 24W was blown, resulting in a value of  $R_{293} = (0.71 \pm 0.06)\Omega$ . The large error associated with this method is due to the response time of the meter and the human adjustment sensitivity. Nonetheless, this directly depends on the precise rating of fuse used, so we take an average of both methods, giving a final value of  $R_{293} = (0.96 \pm 0.09)\Omega$ .

By controlling the input current, a value of  $T$  can be extracted. This corresponds to the electrical Filament Resistance Temperature. To calculate the optical temperature, corresponding to the brightness of the Blackbody Radiation, a correction curve from [5], which is linear in the range of  $T = [1, 2.5] \times 10^3\text{K}$  is applied.

At each value of  $T$ , the optical output  $V$  detected by the photodetector can be measured and a plot of  $\ln(V)$  against  $1/T$  can be used to determine Planck's constant.

## V. RESULTS

We obtained the voltage response using an amplification of 70dB and recorded the resistance of the filament at which no current was flowing through the two branches. This value was used to find the filament's temperature through two conversion procedures outlined above. The investigation was done for each of the 5 narrowband filters and our results are visualised in Fig. 8.

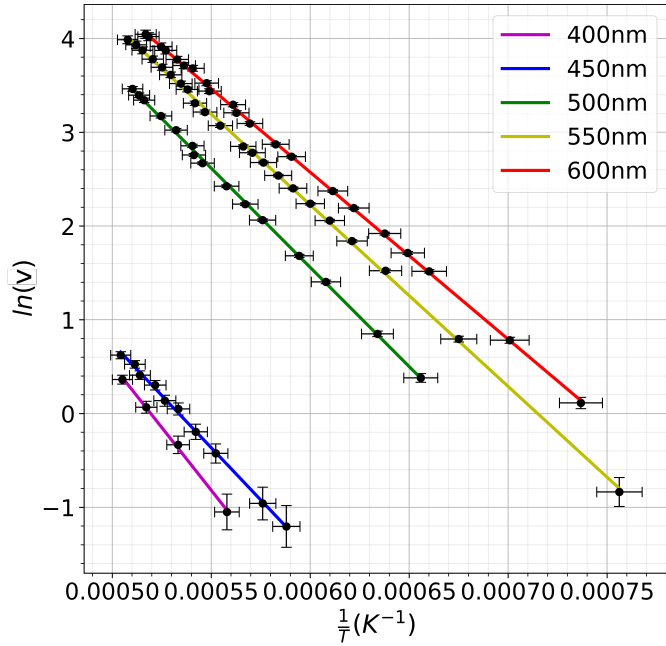


**Fig. 8: Photodetector response with temperature of tungsten lamp:** Plot showing the variation of  $\ln(V)$  against  $1/T$  for each of the 5 filters. The gradient corresponds to  $hc/\lambda_0 K_B$  from (5), from which the value of  $h$  can be extracted.

The gradients of the figure were used to extract  $h$  using (5). These are encapsulated in Table II. These have an average value of  $h = (4.84 \pm 0.13) \times 10^{-34}\text{Js}$ , where the error is the mean of the variances.

Colour	$h \pm \delta h (10^{-34}\text{Js})$
Red	$4.92 \pm 0.08$
Yellow	$4.90 \pm 0.09$
Green	$4.90 \pm 0.10$
Blue	$4.61 \pm 0.13$
Violet	$4.93 \pm 0.20$

**TABLE II: Planck constant values:** Table with the final values of  $h$  and their associated uncertainty, for each of the 5 narrowband filter. The error was calculated using propagation of errors from each individual value, and the least-square fit (Fig. 8). For multiple runs of the same filter, an average value for  $h$  and its associated propagated uncertainty is calculated.

### A. Filament shape

Initially, the iris size was reduced to restrict the proportion of the filament's light that reached the detector (focusing on its hot centre). This was hard to achieve and couldn't be quantified, as the filaments projection wasn't visualised.

We instead decided to use a CMOS camera. We recorded the focused light reaching this detector and found the elliptical average from the centre of the image. We plotted this gaussian variation at multiple temperatures, for each filter. Finally, the FWHM of these distributions is found, which is proportional to the characteristic length  $z(T)$ . This is plotted as a function of temperature in Fig. 9.

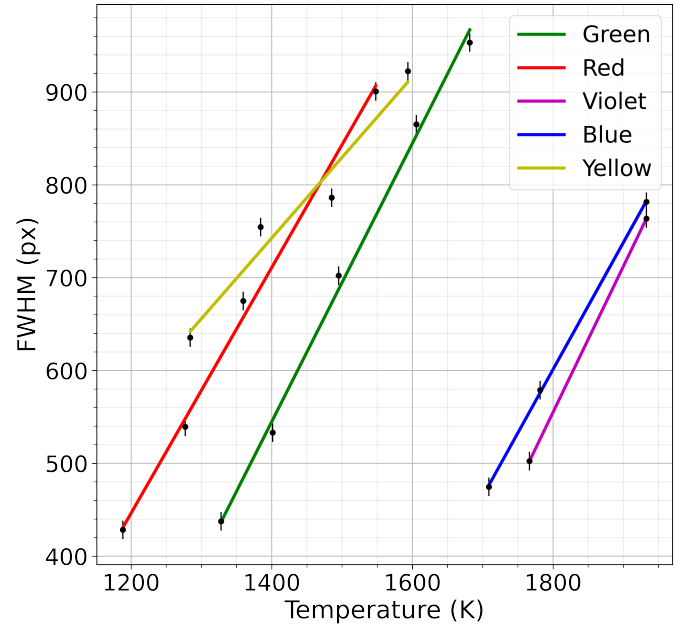


**Fig. 9: FWHM of CMOS light distribution:** FWHM of the projected filament (in units of pixels) shape on the CMOS camera. This value is  $\propto z(T)$ .

A final linear relationship for the characteristic length is extracted from the mean and standard error of the gradients;

$$z(T) \propto (1.32 \pm 0.11)T + B(\lambda) \quad (8)$$

where  $B(\lambda)$  is a constant, dependent on the wavelength of the filter. The exact (positive) proportionality constant to convert pixels into SI units and determine  $z(T)$  is not known in this

investigation. However, we see the filament heating up from the centre, slowly spreading along its length as the temperature increases. This hints that our values of  $h$  are underestimates, as the filament is actually emitting at a lower  $T$  than expected from its measured resistance.

## VI. DISCUSSION

### A. Filament

The non-uniformity of the filament temperature along its length has been determined in (8). The positive gradient means that the wire fuses at the hottest part, making the filaments' linear resistance non-uniform and lowering its average temperature to less than its melting-point value, creating a systematic offset in our results. These regions of the filament will dominate the intensity spectrum, due to the exponential dependence in (1). This part of the investigation could be improved, by attempting to model the light emission from the filament outside of the optical setup, as done in [9]. This could allow us to extract an exact relationship for  $z(T)$ , for which our values for  $T$  could be modified, increasing  $h$ .

### B. Resistances

The first method of determining  $R_{293}$  overly estimated its value. Nonetheless, there was no way to check if the temperature of the filament remained at 293K since it doesn't emit in the visible range at this temperature.

The second (blow-up) method, provided a much lower, accurate value. However, as this method requires destroying lab equipment, only one run was carried out. This could be a significant source of error in the investigation, as it plays a huge role in deriving  $h$ . Recent studies suggest that a slight shift in the value  $R_{293}$  can introduce a systematic error of at least 1% [12] [13].

The errors for the resistances in the Wheatstone bridge are likely underestimates. This method of determining resistances can be improved by employing a Kelvin double bridge [14]; especially for low values of  $R < 1\Omega$ , where the contact resistances become significant.

### C. Measurements and detector response

Care was taken to fix the photodetector in its linear response region (see Section IV-A). However, due to the variational nature of the refractive index of the bi-convex lens with wavelength, the focal length will not be the same for each of the 5 filtered wavelengths; as the refractive index varies inversely with wavelength. As a result of the angular dispersion from the filament, the focal length will be longer for the red light, relative to violet (i.e.  $f(\lambda) \propto 1/\lambda$ ). This will have introduced a small systematic error in each run, as the setup should have been calibrated differently with each filter. Given additional time, we could simulate the path rays shown in Fig. 2 to quantify these chromatic aberrations. To fix the focal length in future investigations, a flint glass can be attached to the lens to make an achromatic doublet [15]. This could also be used to assess the impact of the second order diffraction of light.

The amplification of the detector was fixed throughout the experiment, however, it is still expected that it could have still added different noises, 'dark' currents and varied the non-linearity of the opamp [6].

The photodetector is also sensitive in the infrared range ( $1 < \lambda < 1.1\mu\text{m}$ , introducing additional noise from the lab room. Nonetheless, the scarce presence of these wavelengths at room temperature should make this effect negligible, in comparison to the other sources of error from the detector.

Additionally, its quantum efficiency could also play a role, as there could be a smaller detector response than expected for the given number of photons received. Biesiadzinski et al. [16] find a 4% error in  $V$  using a *HAWAII* – 2RG1.7 $\mu\text{m}$  detector.

### D. Planck's constant

Given the precision of our detector, it was easier to measure and precisely obtain more data values for longer wavelengths. This is seen in Table II, as the errors in our values for blue and violet are 31% and 55% larger than the average error for smaller wavelengths.

Nonetheless, the data values for these filters were mainly gathered in the high-temperature regime of the tungsten emission spectrum; where it is expected that the filament light distribution is more uniform, as the FWHM is larger. However, our errors in this range are larger due to the resistance-temperature relation in Fig. 6.

Between readings, a period of  $\sim 30\text{s}$  was set to allow the filament to reach a steady state. This reduces the bias induced by the direction of the sweep, as preliminary data showed that doing either run at a faster pace gives a percentage difference of as much as 5% for  $h$ . Alternating the direction of the run should average out this error.

## VII. CONCLUSION

The spectral radiance for a Tungsten filament lamp has been investigated for five different wavelengths in the visible spectrum;  $(560 \pm 8)\text{nm}$ ,  $(552 \pm 11)\text{nm}$ ,  $(500 \pm 8)\text{nm}$ ,  $(457 \pm 10)\text{nm}$  and  $(400 \pm 9)\text{nm}$ . A Silicon Amplified Photodetector has been used to record measurements in the temperature range of emission of  $[1, 2] \times 10^3\text{ K}$ , which was found indirectly through a Wheatstone bridge setup. We modelled the filament lamp as a blackbody, and using Planck's law, values for  $h$  have been extracted. An average value in the respectable range of  $h = 4.84 \pm 0.13 \times 10^{-34}\text{Js}$  is obtained. This value is 27% lower than the theoretical value of  $h = 6.626 \times 10^{-34}\text{Js}$ .

We have precisely calibrated the setup and have performed some rigorous error analysis. Empirical modelling of the light distribution of the wire suggests that our values of  $h$  are underestimated, due to the non-uniform heat distribution along the length of the filament. We are motivated to propose further experiments, that could quantify the deviation in  $h$ .

## APPENDIX A THE BLOW-UP METHOD

Extracting the value of  $R_{293}$  using the bulb-blowing method was done by slowly increasing the power supply and recording

it using a camera. The blow-up values obtained are  $I = 1.283\text{A}$  and  $V = 24.599$ . Using the following equation from [12]

$$R_{293} = \frac{R}{(1 + \alpha T + \beta T^2)} \quad (9)$$

a value for  $R_{293}$  can be extracted. Where  $R = V/I$ , and  $\alpha = 5.24 \times 10^{-3}\text{K}^{-1}$  and  $\beta = 0.7 \times 10^{-6}\text{K}^{-2}$  are constants dependant on the properties of tungsten.

## APPENDIX B IMAGE PROCESSING

The CMOS camera recorded the light emitted from the tungsten filament lamp, as a .tiff image. The information was converted into a .txt file and visualised in *Python* using *Matplotlib*. An example of one of the images processed is shown in Fig. 10.

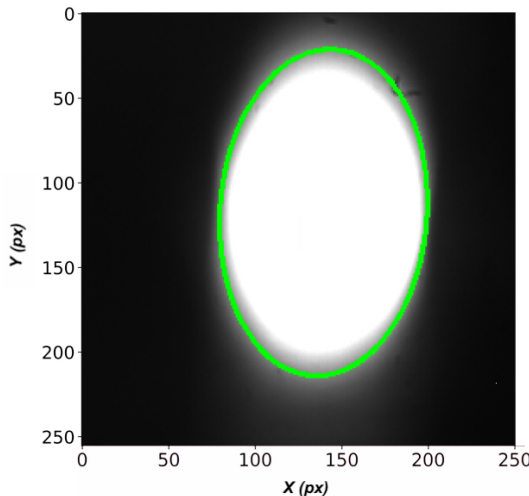


**Fig. 10: Image processing of tungsten filament lamp:** Tungsten emission of red light at  $T = 1190\text{K}$  obtained using a CMOS camera. This image is resized and plotted in a grey-scale. An ellipse is fitted along its edges and is shown in green.

This analysis was automated to allow for a higher volume of images to be processed. This was done using an *OpenCV* library [17]. Firstly, the image was reformatted into a square and a grey-scale. *FindContours()* was used to extract the edges of the light spot. Additionally, we created a function that returned ellipse parameters, given a set of data. The ellipse was then rescaled back into the size of the original image.

## APPENDIX C ERROR PROPAGATION

In a linear approximation, assuming the errors are uncorrelated, we can just apply the propagation of errors formula to a function  $f(x_i)$  [18]

$$\sigma_f^2 = \sum_i \left( \frac{\partial f}{\partial x_i} \right)^2 \sigma_{x_i}^2. \quad (10)$$

The final uncertainty on  $f$  is dependent on the error of its parameters  $\sigma_{x_i}$ .

Equation (10) is used to propagate all the uncertainties throughout this investigation to obtain an error for  $T$ . This includes the error from the resistances ( $R_2$ ,  $R_3$ ,  $R_4$ ) from their specification ( $\sim 1\%$ ), and the two calibrations for  $T(R)$ ; from Fig. 6 and the  $T$  correlation relation from [5]. The errors for  $V$  are obtained using the voltmeters specification.

The error from the fit is extracted using a least-squares weighted fit  $\sigma_m$ , the uncertainty in  $h$  is then determined using

$$\sigma_h = \frac{\lambda_0 k_B}{c} \cdot \sigma_m. \quad (11)$$

Finally, the errors in the fundamental constants ( $k_B$ ,  $c$ ) were considered negligible.

## APPENDIX D FEEDBACK FROM PREVIOUS CYCLES

### A. Cycle 1

**Experiment: Astronomical Imaging.** Grade: 76%. **Marker Summary Comments:** Quality of the graphs and visuals on slide used in the presentation were very good and the presentation benefitted from their inclusion. Structure was good. Delivery occasionally halting and sometimes felt a bit rushed, though technical problems did not help. Good depth of description about their own algorithm, with images to help explain the steps used. Some details of the methods not covered e.g. how elliptical fits and fake sources were established.

### B. Cycle 2

**Experiment: Waves on Strings.** Grade: 77%. **Marker Summary Comments:** Excellent structure and text flow. Good understanding of both theory and the experiment. Extraction of  $E$  not clearly demonstrated and did not consider boundary condition in wound/unwound case. -Excellent use of English language. The figure was pixelised, it's better to use vector images. Should discuss your findings in terms of the model in equation of motion. It would be better to include a figure displaying the setup instead of just describing it via text. Some of the results could be presented in a graph form instead of a Table.

## ACKNOWLEDGMENT

I would like to thank my lab partner since year 1.

## REFERENCES

- [1] G. Kirchhoff, "On the relation between the radiating and absorbing powers of different bodies for light and heat," *The London, Edinburgh, and Dublin Philosophical Magazine and Journal of Science.*, vol. 20, no. 109, pp. 275–301, 1860.
- [2] H. Kragh, *Quantum Generations: A History of Physics in the Twentieth Century*. Princeton University Press, 2002.
- [3] M. Planck, "On the law of distribution of energy in the normal spectrum," *Verhandlungen der Deutschen Physikalischen Gesellschaft*, pp. 237– 245, 1901. [Online]. Available: <https://doi.org/10.1002/andp.19013090310>
- [4] K. I. Kellermann, "Radio source," *Encyclopedia Britannica*, 2021. [Online]. Available: <https://www.britannica.com/science/radio-source>
- [5] P. M. Damzen, "Radiation laws a2," 3rd Year Lab Module. Revised September 2021. Photonics Group, Physics Department, Imperial College London.

- [6] A. Corrons, *Photodetector Calibration*. Dordrecht: Springer Netherlands, 1995, pp. 441–451. [Online]. Available: [https://doi.org/10.1007/978-94-011-0035-9\\_22](https://doi.org/10.1007/978-94-011-0035-9_22)
- [7] C. de Izarra and J.-M. Gitton, “Calibration and temperature profile of a tungsten filament lamp,” *European Journal of Physics*, vol. 31, no. 4, pp. 933–942, jun 2010. [Online]. Available: <https://doi.org/10.1088/0143-0807/31/4/022>
- [8] A. G. Worthing and W. E. Forsythe, “Some effects of diffraction on brightness measurements made with the holbornkurlbaum optical pyrometer,” *Phys. Rev.*, vol. 4, pp. 163–176, Sep 1914. [Online]. Available: <https://link.aps.org/doi/10.1103/PhysRev.4.163>
- [9] L. Fu, R. Leutz, and H. Ries, “Physical modeling of filament light sources,” *Journal of Applied Physics*, vol. 100, pp. 103 528–103 528, 11 2006.
- [10] T. Labs. Quartz tungsten-halogen lamp. [Online]. Available: [https://www.thorlabs.com/newgroupage9.cfm?objectgroup\\_ID=7541](https://www.thorlabs.com/newgroupage9.cfm?objectgroup_ID=7541)
- [11] E. Pawłowski, “Resistivity of tungsten as a function of temperature,” elektron. [Online]. Available: [http://elektron.pol.lublin.pl/elekp/instrukcje\\_LV/Tungsten\\_resistance.pdf](http://elektron.pol.lublin.pl/elekp/instrukcje_LV/Tungsten_resistance.pdf)
- [12] SSERC. Determination of planck’s constant using a tungsten filament lamp. [Online]. Available: [https://www.sserc.org.uk/wp-content/uploads/2014/02/Plancks\\_Constant\\_Tungsten\\_Lamp.pdf](https://www.sserc.org.uk/wp-content/uploads/2014/02/Plancks_Constant_Tungsten_Lamp.pdf)
- [13] H. M. J. P. D. Desai, T. K. Chu and C. Y. Ho, “Electrical resistivity of selected elements,” *Journal of Physical and Chemical Reference Data*, vol. 13, no. 4, pp. 1069–1096, oct 2009. [Online]. Available: <https://doi.org/10.1063/1.555723>
- [14] A. GEORGE, “Kelvin bridge,” Circuit Globe, online. [Online]. Available: <https://circuitglobe.com/kelvin-bridge.html>
- [15] ProfessorMichaelDamzen, “Optics notes - chromatic aberrations,” Imperial College London, year 1 Physics notes.
- [16] T. Biesiadzinski, W. Lorenzon, M. Schubnell, G. Tarlé, and C. Weaverdyck, “Nir detector nonlinearity and quantum efficiency,” *Publications of the Astronomical Society of the Pacific*, vol. 126, no. 937, pp. 243–249, 2014. [Online]. Available: <http://www.jstor.org/stable/10.1086/675735>
- [17] G. Bradski, “The OpenCV Library,” *Dr. Dobb’s Journal of Software Tools*, 2000.
- [18] M. Richards, “Second year statistics of measurement - lecture 5. error propagation.” Imperial College London, year 1 Physics notes.